DOI: 10.1002/adma.200701372

Sol-Gel Inks for Direct-Write Assembly of Functional Oxides**

By *Eric B. Duoss*, *Mariusz Twardowski*, and *Jennifer A. Lewis**

The ability to pattern oxide structures at the microscale in both planar and three-dimensional forms is important for a broad range of emerging applications, including sensors,[1–3] micro-fuel cells[4,5] and batteries,[6,7] photocatalysts,[8,9] solar arrays,[10,11] and photonic bandgap (PBG) materials.[12,13] Here, we report the fabrication of micro-periodic oxide structures by direct-write assembly of sol-gel inks. Specifically, we create both planar and three-dimensional (3D) architectures composed of submicron features, which are converted to the desired oxide phase upon calcination. Atomic force microscopy (AFM) and optical reflectivity measurements acquired on these micro-periodic structures reveal their high degree of structural uniformity.

Several techniques have recently been introduced for patterning materials, including colloidal self-assembly,[14] holographic lithography,[15,16] and direct laser[17,18] and ink writing[19–21] approaches. Unfortunately, these approaches, apart from two notable exceptions,[22,23] are confined to polymeric systems that lack the specific functionality required for a given application. As a consequence, the as-patterned structures require additional processing step(s) to produce the desired functional replicas. For example, 3D micro-fuel cells[24] and photonic bandgap materials[12,13,25,26] with inverse face centered cubic (fcc) structures have been templated from colloidal crystals, while silicon photonic crystals in both normal and inverse woodpile architectures have been templated from polymer structures produced by direct laser[27] and ink[28,29] writing, respectively.

To circumvent the need for complicated templating schemes, we are developing a family of sol-gel inks that enable the direct ink writing (DIW) of functional oxides at the microscale. DIW is a layer-by-layer assembly technique, in which materials are fabricated in arbitrary planar and 3D forms with lateral dimensions that are two orders of magnitude lower than those achieved by ink-jet printing.[30] Paramount to our approach is the creation of concentrated inks that can be extruded through fine deposition nozzles as filament(s), which then undergo rapid solidification to maintain their shape even as they span gaps in underlying layer(s). Unlike our prior efforts based on polyelectrolyte inks[20,21] that require a reservoir-induced coagulation to enable 3D printing, these new inks can be directly printed in air providing exquisite control over the deposition process (e.g., the ink flow can now be started/stopped repeatedly during assembly).

We first demonstrate this new ink design by creating a sol-gel precursor solution based on a chelated titanium alkoxide, titanium diisopropoxide bisacetylacetonate (TIA). TIA has an octahedral coordination of two isopropoxide and two acetylacetone (acac) groups about a central titanium (Ti) atom (Fig. 1a). This molecular structure is ideal, as it leads to the formation of soluble linear chains upon hydrolysis and condensation of the labile isopropoxide groups in the presence of a base catalyst.[31] Subsequent slow hydrolysis of the acac groups leads to further gelation, which when coupled with solvent evaporation, results in the formation of a concentrated ink (Fig. 1b). An organic polymer, polyvinyl-pyrrolidone (PVP), is also incorporated to mitigate stresses that occur during drying and calcination of the as-patterned structures.

We tailor the ink viscosity for DIW through micron-sized nozzles by regulating the solids content, defined as Ti + PVP concentration (wt %). The initial precursor solution contains 6.6 wt % solids and possesses a low viscosity ~0.01 Pa·s, as shown in Figure 1c. However, upon concentrating the ink via solvent evaporation, a dramatic rise in viscosity is observed. For example, a nearly four-fold increase in ink concentration leads to a three orders of magnitude rise in its viscosity. Using an approximation of the Hagen–Poiseuille model,[21] we estimate that the optimal ink viscosity ranges from 2.1–4.2 Pa·s for the DIW conditions employed in this study (i.e., 1 μm deposition nozzle, 400 μm s^{-1} deposition speed, and an applied pressure of 275–550 kPa). There is good agreement between the predicted values and those deemed optimal experimentally for microscale printing, as highlighted by the shaded region in Figure 1c. These inks not only flow readily, but are concentrated enough to rapidly solidify and maintain their cylindrical shape upon exiting the nozzle.

The ink solidification mechanism can be understood by examining its elastic (G') and viscous (G'') moduli in the presence and absence of an ethanol solvent trap (Fig. 1d). The as-printed ink exhibits a liquid-like response (i.e., $G'' > G'$). How-

[*] Prof. J. A. Lewis, E. B. Duoss, Dr. M. Twardowski
Department of Materials Science and Engineering, and
Frederick Seitz Materials Research Laboratory
University of Illinois at Urbana-Champaign
Urbana, IL 61801 (USA)
E-mail: jalewis@uiuc.edu

[**] This material is based on work supported by the U. S. Army Research Office under contract/grant number DAAD19-03-1-0227. Partial support was also provided by the U.S. Department of Energy, Division of Materials Sciences, under Award No. DEFG-02-91ER45439, through the Frederick Seitz Materials Research Laboratory at the University of Illinois at Urbana-Champaign, for measurements obtained in the Center for Microanalysis of Materials, University of Illinois. We thank G. Gratson, M. Xu, S. Rhodes, W. Wu, J. Carroll, III, T. Malkowski, F. García-Santamaría, and P. Braun for useful discussions. Supporting Information is available online from Wiley InterScience or from the authors.

ADVANCED MATERIALS

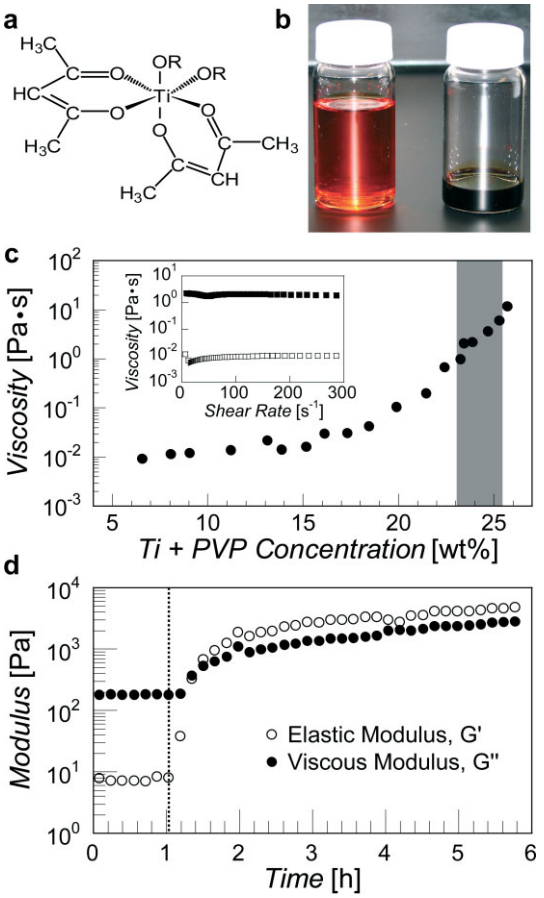

Figure 1. a) Molecular structure of the titania-based precursor used in the sol-gel ink formulation, R = $CH(CH_3)_2$. b) Optical image of the initial precursor solution (left) and ink after solvent evaporation (right). c) Ink viscosity as a function of increasing solids content, defined as Ti + PVP (in wt %). Shaded region indicates printing regime for a 1 μm nozzle. c, inset) Both the initial precursor solution (open squares, Ti + PVP = 6.6 wt %) and printable ink (filled squares, Ti + PVP = 23.4 wt %) exhibit Newtonian flow behavior. d) Elastic and viscous moduli as a function of time in the presence and absence of an ethanol solvent trap. The vertical line denotes when solvent trap is removed thereby exposing the sample to air (t = 1.05 h).

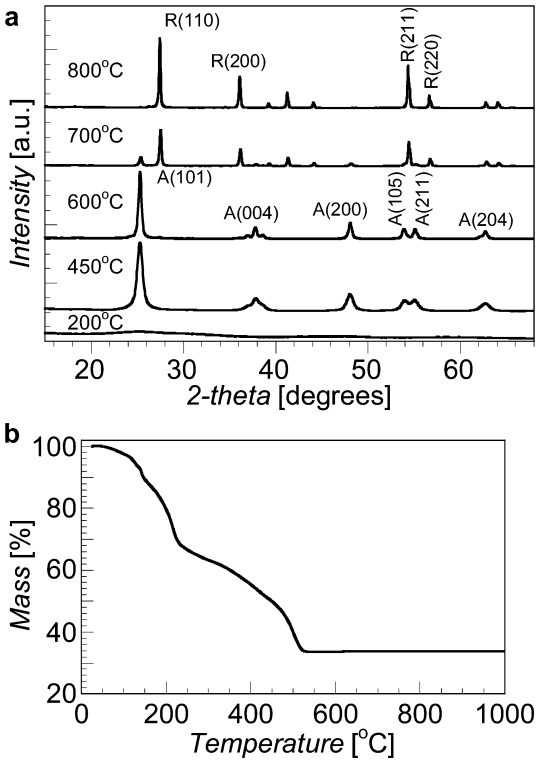

Figure 2. a) X-ray diffraction data obtained after calcining the sol-gel ink to different temperatures to produce the desired oxide phase(s). The peaks are denoted by A (TiO_2 anatase) and R (TiO_2 rutile), where A > 98 wt % at 600 °C and R > 97 wt % at 800 °C. b) Thermogravimetric analysis of the sol-gel ink (23.4 wt % solids).

ever, upon exposure to air (t > 1.05 h), the ink solidifies (i.e., $G' > G''$) as further solvent evaporation occurs. Note, the microscale filaments have a much higher surface area to volume ratio than the rheological samples, hence their solidification occurs at much faster timescales. We estimate that a 1 μm diameter filament solidifies ~10 ms, which is equivalent to the time required for the nozzle to traverse a 4 μm gap between underlying filaments at a build speed of 400 μm s^{-1} in air.

The ink filaments are calcined at elevated temperatures to produce the desired functional oxide phase(s). X-ray diffraction (XRD) shows that peaks characteristic of TiO_2 (anatase) appear at 450 °C (Fig. 2a), whereas phase conversion is nearly complete (> 98 wt %) by 600 °C. Further heating to 800 °C yields the rutile phase (> 97 wt %). Thermogravimetric analysis (TGA) performed on this ink indicates that complete organic decomposition occurs by 525 °C (Fig. 2b), in good agreement with the onset of crystallization. Due to the total mass loss observed (~67 wt %), the as-patterned structures undergo significant volumetric shrinkage during calcination.

We next demonstrate the patterning of 1D micro-periodic arrays composed of parallel ink filaments (or rods) deposited through a 1 μm nozzle. A wide range of print conditions are explored, including varying the rod center-to-center spacing (a) from 2–10 μm and build speed (v) from 400–2000 μm s^{-1}. A representative structure consisting of TiO_2 (anatase) rods built with a = 2 μm and v = 1600 μm s^{-1} is shown in Figure 3a. These filamentary features remain pinned to the substrate surface during calcination; hence, their shrinkage occurs radially. The height profile data, shown in Figure 3b, indicates that the rods have an average width (w) = (268 ± 9) nm, height (h) = (223 ± 9) nm, and a = (1.977 ± 0.077) μm.

To demonstrate that direct-write assembly of sol-gel inks opens a new avenue to functional devices, 3D micro-periodic structures composed of parallel arrays of orthogonally stacked rods are produced. We choose to create a woodpile architecture, because it is well suited for photonic applications.[32,33] Photonic crystals (PCs) possess a photonic bandgap that prohibits the propagation of light within a certain frequency range. TiO_2 is a good candidate material for such applications due to its high refractive index and low absorption in the visible and near infrared spectral regions.[34,35]

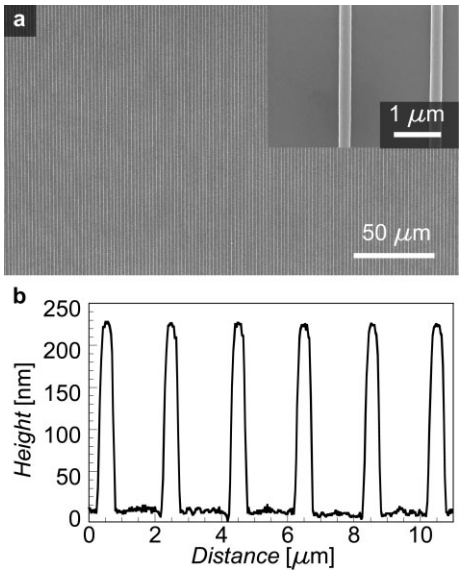

Figure 3. a) Scanning electron microscopy (SEM) images of a 1D-periodic structure (2 mm × 2 mm) composed of parallel TiO_2 rods. The rod width (w) is (268 ± 9) nm and rod center-to-center spacing (a) is (1.977 ± 0.077) μm. b) Height profile of representative features shown in (a), where the average rod height is (223 ± 9) nm.

A representative 3D woodpile structure is shown in Figure 4a (see Supporting Information for a time-lapse video of the patterning process). From the inset, we find that the rods (w = (1.212 ± 0.024) μm) are bonded to one another and span gaps (a = (4.002 ± 0.053) μm) between underlying rods. During calcination, the first layer of these structures is pinned to the substrate surface, but rods in subsequent layers contract both radially and laterally. If the first layer remains constrained throughout this process, the 3D structures experience anisotropic shrinkage that may induce severing of the first layer. To mitigate this problem, the ink is printed onto substrates precoated with a sacrificial organic layer. During calcination, the sacrificial layer melts allowing the patterned 3D structure to first release from the underlying surface prior to shrinking isotropically.

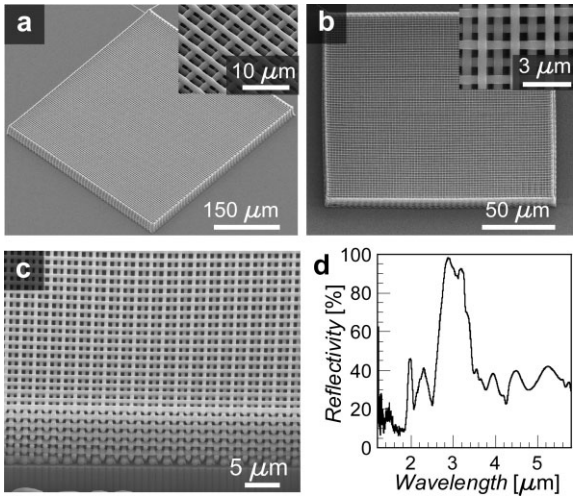

Figure 4. a) SEM image of as-patterned 3D structure (24-layers, w = (1.212 ± 0.024) μm, a = (4.002 ± 0.053) μm) and high magnification inset viewed at 45° tilt. b) SEM image of calcined TiO_2 structure (24-layers, w = (520 ± 6) nm, a = (2.097 ± 0.095) μm) heated to 715 °C, viewed at 45° and a high magnification inset of this structure. c) Focused ion beam (FIB)-milled cross-section of the oxide structure shown in (b). d) Optical reflectivity data of oxide structure shown in (b).

A TiO_2 structure (24-layer) fabricated on this sacrificial layer and calcined to 715 °C is shown in Figure 4b. The final 3D structure possesses an edge length of (157.90 ± 0.98) μm (reduced from its initial value of 300 μm), w = (520 ± 6) nm, and a = (2.097 ± 0.095) μm (reduced from its initial value of 4 μm). From these values, the rod volumetric shrinkage is calculated as 85.8 %, which corresponds to a density of 3.65 g cm^{-1} for the TiO_2 filaments (ρ_{ink} = 1.40 g cm^{-1}). Thus, after calcination, the TiO_2 filaments are ~ 90 % dense (assuming ρ_{TiO_2} = 4.05 g cm^{-1} for fully dense TiO_2). Excellent registration is observed in both the higher magnification image shown in Figure 4b (inset) as well as the focused ion beam (FIB)-milled cross-section shown in Figure 4c. From Figure 4c, the four-layer repeat distance, c, is measured as (1.900 ± 0.090) μm, which yields values of c/a = 0.91 and TiO_2-in-air filling fraction = 0.19. The volumetric shrinkage of the as-patterned structures, and, hence, their optical properties, can be controlled by varying the ink composition (i.e., Ti + PVP wt %). By reducing the Ti/PVP ratio within the patterned structure, the volumetric shrinkage will be enhanced thereby leading to a more pronounced blue-shift in the reflectance peaks after calcination.

The 3D micro-periodic TiO_2 structure displays an exceptionally broad peak width of ~ 26 % (FWHM divided by mid-peak value) and an intense reflectance peak of 98 % at λ = 2.9 μm (Fig. 4d), indicative of a highly ordered structure. These data are acquired from an angle centered around 16.7° with respect to sample normal, which nominally corresponds the Γ-X′ direction for this woodpile structure. The magnitude of the stop-peak is a consequence of the large refractive index (n) contrast between TiO_2 and air. XRD analysis of inks calcined to 715 °C reveal their composition to be a mixture of TiO_2 anatase (47.3 wt %) and rutile (52.7 wt %) phases. Thus, by simple rule of mixtures analysis, the filaments have an approximate n of 2.6 at visible wavelengths, which is well above the theoretical minimum of n = 1.9 required to open a complete PBG in an fcc woodpile (i.e., c/a = 1.414).[32] Calcining at higher temperatures is avoided to prevent significant grain growth and surface roughness that degrade optical properties.[36] A key advantage of DIW fabrication of PCs over colloidal self-assembly and holographic lithography routes is the ability to directly embed functional defects into the as-patterned structures. As stated previously, we can repeatably terminate and re-initiate the flow of these sol-gel inks (see Supporting Information for a time-lapse movie illustrating this process). This advance will ultimately allow the incorporation of functional defects, e.g., 90° bends and point defects; a subject of ongoing efforts.

ADVANCED MATERIALS

In summary, we have developed sol-gel inks for direct-write assembly of micro-patterned oxides in both planar and 3D configurations. The ink rheology has been tailored to facilitate both flow through fine deposition nozzles and solidification in air upon exiting the nozzle. During calcination, the structures are converted into the desired oxide phase, while simultaneously maintaining their structural fidelity even as they experience significant volumetric shrinkage. Our ability to directly pattern functional oxides obviates the need for complex templating schemes, such as biomimetic mineralization[37] or chemical vapor deposition,[27–29] that often amplify imperfections in the underlying structure. Hence, this approach is particularly well suited for the assembly of 3D PCs, whose optical properties are highly sensitive to such imperfections. Equally important, our sol-gel ink design and patterning approach can be readily extended to other organometallic precursors. For example, we have recently formulated inks for microscale patterning of electrically (e.g., doped-TiO_2), transparent (e.g., indium tin oxide), and ionically (e.g., doped-zirconium oxide) conducting oxides. This broad palette of materials will enable a myriad of potential applications to be pursued, including photonics, sensors, photocatalysts, displays, photovoltaics, and fuel cells.

Experimental

Ink Synthesis: Sol-gel inks are prepared by first dissolving 0.31 g of polyvinyl-pyrrolidone (PVP) ($M_w = 55\,000$, Sigma–Aldrich Corporation, St. Louis, MO) in 4 mL of absolute ethanol (EtOH) (200 proof, Aaper Alcohol and Chemical Company, Shelbyville, KY). 6.25 g of titanium diisopropoxide bis(acetylacetonate) (TIA) (75 wt % in 2-propanol, Sigma–Aldrich Corporation, St. Louis, MO) is then added to this polymer solution. Finally, 4 mL of EtOH, 0.93 mL of H_2O, and 0.67 mL of concentrated NH_4OH (~14.1 N) are added to this precursor solution. The solution is heated at 80 °C while stirring for ~12 h to create the desired sol-gel ink. All chemicals are used as-received.

Ink Rheology: The viscosity of the initial precursor solution and those heated to 70 °C for varying times is measured using a stress-controlled rheometer (C-VOR, Malvern Instruments, Malvern UK). Specifically, each solution is placed in a concentric cylinder geometry (C8, bob diameter of 8 mm and an inter-cylinder distance of 0.4 mm) and their viscosity is measured as a function of shear rate (10–300 s^{-1}) in ascending order at a fixed temperature of 25 °C in the presence of an ethanol solvent trap. For each solution, the viscosity measured at an approximate shear rate of 110 s^{-1} is reported as a function of solids loading, defined as the concentration of titanium and PVP (by wt % of solution). Elastic and viscous moduli are measured using an oscillatory technique at a frequency of 1 Hz. The ethanol solvent trap is removed after 1.05 h and the cup and bob geometry is exposed to air. Data are collected for a period of ~6 h.

Ink Characterization: X-ray diffraction (XRD) is used to determine the phase evolution during calcination of the sol-gel ink. Specifically, thick films (~15 μm) are produced by spin-coating. After heating to the desired temperature in air, the film is ground to powder form and analyzed by XRD (D-Max X-ray diffractometer, Rigaku International Corp., Tokyo, Japan). A fixed anode Cu source with monochromatic Kα radiation is used. The crystalline phase composition (wt %) is determined using Jade X-ray analysis software (Materials Data, Inc., Livermore, CA). The ink is also subjected to thermogravimetric analysis (Mettler Toledo TGA/SDTA851, Columbus, OH) to determine the mass loss upon heating to 1000 °C at 10 °C min^{-1} in air.

Direct-Write Assembly: The sol-gel ink (~23.4–25.3 wt % solids, η ~2–6 Pa·s) is housed in a 3 mL barrel (EFD Inc., East Providence, RI) attached by luer-lok to a borosilicate glass micronozzle (diameter = 1 μm, P-2000 laser based micropipette puller, Sutter Instrument Co., Novato, CA). This ink delivery system is mounted on a three-axis micropositioning stage (ABL 900010 *x*-*y*-*z* motion stage, Aerotech, Inc., Pittsburgh, PA) controlled with computer-aided design software (RoboCAD, 3D Inks, Stillwater, OK). An air-powered fluid dispenser (800 ultra dispensing system, EFD Inc.) is connected to the delivery system to pressurize the barrel and control flow rate. The required pressure depends on both the ink viscosity and printing speed, but typically ranged from 275–550 kPa.

Planar structures are patterned on double-polished silicon wafers at a printing speed (v) = 1600 μm s^{-1}. The ink filament diameter is approximately equal to the nozzle size of 1 μm, the center-to-center separation distance (a) between filaments is 2 μm, and the patterned area is 2 mm × 2 mm. 3D micro-periodic structures are patterned onto silicon wafers that are pre-coated with a sacrificial organic layer. This release layer is produced by spin coating a 15 wt % solution of Crystalbond™ 509 (Structure Probe, Inc., West Chester, PA, T_m = 121 °C) dissolved in acetone onto a silicon wafer at 2500 rpm for 60 s (P-6000 spin coater, Integrated Technologies, Inc., Acushnet, MA). Representative 3D micro-periodic structures (24-layer) are created by ink deposition through a 1 μm nozzle with v = 400 μm s^{-1}, a = 4 μm, and a lateral area of 300 μm × 300 μm. All structures are printed directly in air with a relative humidity of 18–35 % at 20–25 °C. After completion, structures are stored in a desiccator until further processing. Note, the characteristic build times for both the planar and 3D structures are approximately 20 min.

The as-patterned structures are calcined in air in a furnace (Lindberg/Blue M 894, Thermo Electron Corp., Asheville, NC) to form the desired oxide phase. For 1D micro-periodic structures, a heating profile of 2 °C min^{-1} to 515 °C, 1 h hold, 5 °C min^{-1} to 615 °C, 1 h hold is used, whereas the multilayer structures are heated at 2 °C min^{-1} to 515 °C, 1 h hold, 5 °C min^{-1} to 715 °C, 1 h hold followed by furnace cooling.

Structural Characterization: Scanning electron microscopy (SEM) images are obtained on the as-patterned and calcined micro-periodic structures using a Hitachi S-4700 scanning electron microscope (Hitachi, Ltd., Tokyo, Japan). Cross-sectional images of the calcined 3D micro-periodic structures are obtained by first sectioning them using focused ion beam milling (Strata DB 235 FIB, FEI Co., Hillsboro, OR).

To probe the structural uniformity of the 1D micro-periodic structures, their height profiles are generated using contact-mode, atomic force microscopy (AFM) (Dimension 3100 atomic force microscope, Veeco Instruments, Inc., Woodbury, NY). The ink filament height (h) is obtained from line scans of 84 rods at 10 different locations (8–9 rods in each location). In addition, the rod width (w) is acquired from SEM images (top view) of 60 rods by measuring multiple rods at 15 different locations throughout the sample. The rod center-to-center spacing (a) is determined from 45 measurements taken from the same 15 locations. For the as-patterned 3D micro-periodic structure, 12 measurements (6 each in *x*- and *y*-directions) acquired from SEM images of the top 4 layers are used to obtain w and a values. For the calcined woodpile, 28 measurements (14 in each direction) from SEM images of the top 4 layers were measured from 7 locations to obtain w and a values. The pattern edge length was calculated from 12 measurements (6 in each direction), all from distinct locations. Values for the four-layer repeat distance (c) are acquired from a high magnification FIB cross-section (not shown) by measuring 8 locations and taking into account the tilt angle (52.4°). For each measurement, the values are averaged and the standard deviation is calculated.

Optics: A Fourier-transform infrared spectrometer (FTIR) (Bruker Vertex 70, globar lamp, Billerica, MA) combined with an infrared microscope (Bruker Hyperion 2000) and liquid nitrogen cooled InSb detector are used to acquire reflectivity spectra. 3D micro-periodic structures are measured with a 15× Cassegrain objective (numerical aperture = 0.4) that probes the sample surface at an angle centered about 16.7° with respect to sample normal. A circular aperture is

placed in the image plane, which allows selection of a 20 μm diameter region of the sample. Reflectivity spectra are normalized to a gold mirror. In order to avoid edge effects, the center areas of the sample are measured and no significant variations in optical performance are observed within these regions of the sample.

Received: June 7, 2007
Revised: July 27, 2007
Published online: ■

[1] Z. W. Pan, A. R. Dai, Z. L. Wang, *Science* **2001**, *291*, 1947.
[2] O. K. Varghese, D. Gong, M. Paulose, K. G. Ong, E. C. Dickey, C. A. Grimes, *Adv. Mater.* **2003**, *15*, 624.
[3] I.-D. Kim, A. Rothschild, B. H. Lee, D. Y. Kim, S. M. Jo, H. L. Tuller, *Nano Lett.* **2006**, *6*, 2009.
[4] B. C. H. Steele, A. Heinzel, *Nature* **2001**, *414*, 345.
[5] C. D. Baertsch, K. F. Jensen, J. L. Hertz, H. L. Tuller, S. T. Vengallatore, S. M. Spearing, M. A. Schmidt, *J. Mater. Res.* **2004**, *19*, 2604.
[6] B. T. Holland, C. F. Blanford, A. Stein, *Science* **1998**, *281*, 538.
[7] R. W. Hart, H. S. White, B. Dunn, D. R. Rolison, *Electrochem. Commun.* **2002**, *5*, 120.
[8] M. R. Hoffmann, S. T. Martin, W. Choi, D. W. Bahnemann, *Chem. Rev.* **1995**, *95*, 69.
[9] A. L. Linsebigler, G. Lu, J. T. Yates, Jr., *Chem. Rev.* **1995**, *95*, 735.
[10] B. O'Regan, M. A. Grätzel, *Nature* **1991**, *353*, 737.
[11] M. Grätzel, *Nature* **2001**, *414*, 338.
[12] Y. Xia, B. Gates, Y. Yin, Y. Lu, *Adv. Mater.* **2000**, *12*, 693.
[13] C. López, *Adv. Mater.* **2003**, *15*, 1679.
[14] A. D. Dinsmore, J. C. Crocker, A. G. Yodh, *Curr. Opin. Colloid Interface Sci.* **1998**, *3*, 5.
[15] D. Mei, B. Cheng, H. Wei, L. Zhaolin, Z. Daozhong, *Opt. Lett.* **1995**, *20*, 429.
[16] M. Campbell, D. N. Sharp, M. T. Harrison, R. G. Denning, A. J. Turberfield, *Nature* **2000**, *404*, 53.
[17] B. H. Cumpston, S. P. Anathavel, S. Barlow, D. L. Dyer, J. E. Ehrlich, L. L. Erskine, A. A. Heikal, S. M. Kuebler, I.-Y. Sandy Lee, D. McCord-Maughon, J. Qin, H. Rockel, M. Rumi, X.-L Wu, S. R. Marder, J. W. Perry, *Nature* **1999**, *398*, 51.
[18] M. Deubel, G. von Freymann, M. Wegener, S. Pereira, K. Busch, C. M. Soukoulis, *Nat. Mater.* **2004**, *3*, 444.
[19] J. A. Lewis, G. M. Gratson, *Mater. Today* **2004**, *7–8*, 32.
[20] G. M. Gratson, M. Xu, J. A. Lewis, *Nature* **2004**, *428*, 386.
[21] G. M. Gratson, J. A. Lewis, *Langmuir* **2005**, *21*, 457.
[22] S. Wong, M. Deubel, F. Perez-Willard, S. John, G. A. Ozin, M. Wegener, G. von Freymann, *Adv. Mater.* **2006**, *18*, 265.
[23] S. Passinger, M. S. M. Saifullah, C. Reinhardt, K. R. V. Subramanian, B. N. Chichkov, M. E. Welland, *Adv. Mater.* **2007**, *19*, 1218.
[24] H. Yan, C. F. Blanford, B. T. Holland, M. Parent, W. H. Smyrl, A. Stein, *Adv. Mater.* **1999**, *11*, 1003.
[25] O. D. Velev, A. M. Lenhoff, *Curr. Opin. Colloid Interface Sci.* **2000**, *5*, 56.
[26] A. Stein, R. C. Schroden, *Curr. Opin. Solid State Mater. Sci.* **2001**, *5*, 553.
[27] N. Tetreault, G. von Freymann, M. Deubel, M. Hermatschweiler, F. Perez-Willard, S. John, M. Wegener, G. A. Ozin, *Adv. Mater.* **2006**, *18*, 457.
[28] G. M. Gratson, F. García-Santamaría, V. Lousse, M. Xu, S. Fan, J. A. Lewis, P. V. Braun, *Adv. Mater.* **2006**, *18*, 461.
[29] F. García-Santamaría, M. Xu, V. Lousse, S. Fan, P. V. Braun, J. A. Lewis, *Adv. Mater.* **2007**, *19*, 1567.
[30] P. Calvert, *Chem. Mater.* **2001**, *13*, 3299.
[31] A. Yamamoto, S. Kambara, *J. Am. Chem. Soc.* **1957**, *79*, 4344.
[32] K.-M. Ho, C. T. Chan, C. M. Soukoulis, R. Biswas, M. Sigalas, *Solid State Commun.* **1994**, *89*, 413.
[33] H. S. Sözüer, J. P. Dowling, *J. Mod. Opt.* **1994**, *41*, 231.
[34] G. Subramania, K. Constant, R. Biswas, M. M. Sigalas, K.-M. Ho, *Appl. Phys. Lett.* **1999**, *74*, 3933.
[35] G. Subramanian, V. N. Manoharan, J. D. Thorne, D. J. Pine, *Adv. Mater.* **1999**, *11*, 1261.
[36] X. Z. Ding, Z. A. Qi, Y. Z. He, *Nanostruct. Mater.* **1994**, *4*, 663.
[37] M. Xu, G. M. Gratson, E. B. Duoss, R. F. Shepherd, J. A. Lewis, *Soft Matter* **2006**, *2*, 205.

COMMUNICATIONS

Assembly

Sol-gel inks have been developed for direct-write assembly of functional oxide structures with sub-micron features. Highly uniform, planar and 3D micro-periodic structures (see figure) have been patterned that can be readily converted to titania upon calcination.